Journal of Virology

Cholesterol-Dependent Membrane Fusion Induced by the gp41 Membrane-Proximal External Region–Transmembrane Domain Connection Suggests a Mechanism for Broad HIV-1 Neutralization

Beatriz Apellániz, Edurne Rujas, Pablo Carravilla, José Requejo-Isidro, Nerea Huarte, Carmen Domene and José L. Nieva

***J. Virol.* 2014, 88(22):13367. DOI: 10.1128/JVI.02151-14.**
Published Ahead of Print 10 September 2014.

JVI Journals.ASM.org

Cholesterol-Dependent Membrane Fusion Induced by the gp41 Membrane-Proximal External Region–Transmembrane Domain Connection Suggests a Mechanism for Broad HIV-1 Neutralization

Beatriz Apellániz,[a] Edurne Rujas,[a] Pablo Carravilla,[a] José Requejo-Isidro,[a] Nerea Huarte,[a] Carmen Domene,[b,c] José L. Nieva[a]

Biophysics Unit (CSIC-UPV/EHU) and Department of Biochemistry and Molecular Biology, University of the Basque Country (UPV/EHU), Bilbao, Spain[a]; Chemistry Research Laboratory, University of Oxford, Oxford, United Kingdom[b]; Department of Chemistry, King's College London, London, United Kingdom[c]

ABSTRACT

The HIV-1 glycoprotein 41 promotes fusion of the viral membrane with that of the target cell. Structural, biochemical, and biophysical studies suggest that its membrane-proximal external region (MPER) may interact with the HIV-1 membrane and induce its disruption and/or deformation during the process. However, the high cholesterol content of the envelope (ca. 40 to 50 mol%) imparts high rigidity, thereby acting against lipid bilayer restructuring. Here, based on the outcome of vesicle stability assays, all-atom molecular dynamics simulations, and atomic force microscopy observations, we propose that the conserved sequence connecting the MPER with the N-terminal residues of the transmembrane domain (TMD) is involved in HIV-1 fusion. This junction would function by inducing phospholipid protrusion and acyl-chain splay in the cholesterol-enriched rigid envelope. Supporting the functional relevance of such a mechanism, membrane fusion was inhibited by the broadly neutralizing 4E10 antibody but not by a nonneutralizing variant with the CDR-H3 loop deleted. We conclude that the MPER-TMD junction embodies an envelope-disrupting C-terminal fusion peptide that can be targeted by broadly neutralizing antibodies.

IMPORTANCE

Fusion of the cholesterol-enriched viral envelope with the cell membrane marks the beginning of the infectious HIV-1 replicative cycle. Consequently, the Env glycoprotein-mediated fusion function constitutes an important clinical target for inhibitors and preventive vaccines. Antibodies 4E10 and 10E8 bind to one Env vulnerability site located at the gp41 membrane-proximal external region (MPER)–transmembrane domain (TMD) junction and block infection. These antibodies display broad viral neutralization, which underscores the conservation and functionality of the MPER-TMD region. In this work, we combined biochemical assays with molecular dynamics simulations and microscopy observations to characterize the unprecedented fusogenic activity of the MPER-TMD junction. The fact that such activity is dependent on cholesterol and inhibited by the broadly neutralizing 4E10 antibody emphasizes its physiological relevance. Discovery of this functional element adds to our understanding of the mechanisms underlying HIV-1 infection and its blocking by antibodies.

The HIV-1 envelope glycoprotein (Env) embodies a class I fusion machinery (1–3). The Env complex is organized at the surface of the infectious virus mostly as a trimer of noncovalently associated heterodimers (4, 5). Each heterodimer is generated upon cleavage of the gp160 precursor by furin-like proteases, giving rise to the two composing subunits, gp120 (surface) and gp41 (transmembrane), which mediate receptor binding and virus-cell fusion, respectively (4). Recent structural studies confirm that in the prefusion, native state, interprotomer association is primarily mediated by hydrophobic contacts between gp120 subunits and a preformed trimeric coiled-coil domain involving the N-terminal (NHR) gp41 helices (6–8). Other regions, such as the gp120 V1-V3 variable loops and the membrane-proximal external region (MPER) of gp41, also contribute to stabilize the complex, but to a lesser extent (9, 10).

The model displayed in Fig. 1A highlights three states within the most widely accepted mechanism of virus-cell membrane fusion induced by the Env glycoprotein (3, 4, 11, 12). Upon receptor/coreceptor engagement, the native gp120 trimer (state I) acquires an open configuration, and it is thought to transmit conformational signals to gp41, most likely through the C1/C5 regions, which activates the fusion cascade. Two distinct gp41 structural elements take part in the subsequent steps of the process: (i) membrane-inserting domains, namely, the fusion peptide (FP) and the membrane-proximal external region (MPER)–transmembrane domain (TMD) region, which anchor gp41 in the prehairpin configuration (state II) to target cell and viral membranes, respectively, and (ii) helical domains NHR and CHR, which assemble into an energetically stable 6-helix bundle (6-HB) or hairpin (state III). It is assumed that completion of the 6-HB structure results in the relocation of the FP and MPER/TMD into spatial proximity, thereby enabling anchored membranes to merge (12, 13).

However, close apposition of membranes pulled together by a growing 6-HB is hampered by the strong, repulsive hydration and electrostatic forces operating at their surfaces, which consequently prevent the initial mixing of their lipid constituents (11, 14, 15). Thus, it has been argued that, beyond the anchoring effect, the

Received 22 July 2014 **Accepted** 2 September 2014
Published ahead of print 10 September 2014
Editor: F. Kirchhoff
Address correspondence to Carmen Domene, carmen.domene@chem.ox.ac.uk, or Jose L. Nieva, joseluis.nieva@ehu.es.

doi:10.1128/JVI.02151-14

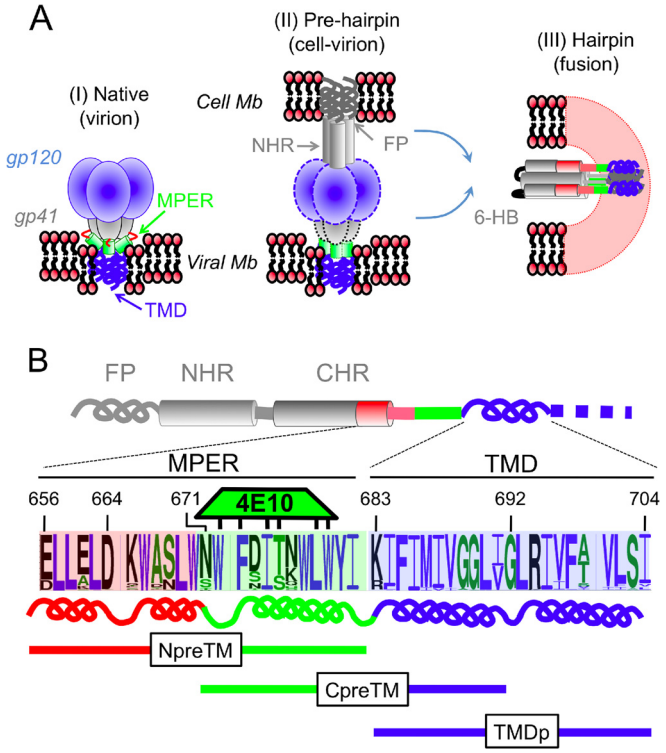

FIG 1 Proposed model for HIV-1 Env-induced membrane fusion (A) and designation of the gp41 MPER-TMD region (B). The highlighted gp41 elements are as follows: FP, fusion peptide; NHR and CHR, amino- and carboxy-terminal helical regions, respectively; MPER, membrane-proximal external region; TMD transmembrane domain; 6-HB: 6-helix bundle. In panel B, MPER-TMD sequence variability within HIV-1 clade B is displayed as a WebLogo representation (75). Nonpolar amino acids are in blue. The green box above indicates the position of the 4E10 epitope. The tick marks indicate residues facing the paratope with helical periodicity. The diagram under the sequence delimits the helical subdomains and locates positions for nonhelical junctions. Bars below the helices span the sequences covered by the overlapping peptides used in this study.

N-terminal FP inserted into the target membrane could generate the focal points of dehydration and hydrophobic destabilization required for fusion (recently reviewed in reference 14). Complementarily, it has been suggested that shallow insertion of MPER into the envelope external leaflet might prime the opposing viral membrane for fusion (16–19). Supporting its conservation and functionality, the MPER comprises one of the four "sites of vulnerability" targeted by broadly neutralizing antibodies within the Env glycoprotein and the only one existing within the gp41 subunit (reviewed in references 20 and 21). Interestingly, among the anti-MPER antibodies identified so far, 4E10 and 10E8 are the most broadly reactive, and both bind to residues spanning the MPER-TMD junction (22, 23).

The viral membrane is enriched in cholesterol (Chol), its content reaching ca. 50 mol% (24–26). The high rigidity imparted by this compound accumulated in the viral envelope is predicted to oppose the deformations required for fusion (11, 15). Thus, here we sought to establish whether a sequence with the capability of perturbing and fusing highly rigid membranes would exist within the gp41 MPER-TMD region. To that aim, we designed three overlapping peptides spanning residues 656 to 704 (HXB2c numbering) (Fig. 1B). Functional characterization in a lipid vesicle system demonstrated that peptides representing the MPER sequence (NpreTM) or the TMD (TMDp) barely induced fusion under any condition. In contrast, the CpreTM peptide covering the MPER-TMD junction was a Chol-dependent fusogenic sequence which displayed significant activity at concentrations of this compound comparable to those existing at the viral envelope. Molecular dynamics simulations (MDS) in conjunction with atomic force microscopy (AFM) provided insights into the possible mechanism underlying the CpreTM fusogenic activity measured *in vitro* and its dependence on cholesterol. Furthermore, emphasizing the physiological relevance of the detected activity, CpreTM-induced fusion was inhibited by the functional 4E10 antibody but not by a nonneutralizing version with the CDR-H3 tip deleted. These findings suggest that neutralizing antibodies binding to the MPER C terminus might block infection by targeting the fusogenic function of the MPER-TMD junction.

MATERIALS AND METHODS

Materials. The peptides used in this study, NEQELLELDKWASLWNWF NITNWLWYIK (NpreTM), KKK-NWFDITNWLWYIKLFIMIVGGLV-KK (CpreTM), KKK-NAADITNWLWYIKLFIMIVGGLV-KK (Cala), and KKK-LFIMIVGGLVGLRIVFAVLSI-KKK (TMDp), were synthesized in C-terminal carboxamide form by solid-phase methods using Fmoc chemistry, purified by reverse-phase high-performance liquid chromatography (HPLC), and characterized by matrix-assisted laser desorption ionization–time-of-flight (MALDI-TOF) mass spectrometry (purity > 95%). Peptides were routinely dissolved in dimethyl sulfoxide (DMSO; spectroscopy grade), and their concentrations were determined by the bicinchoninic acid microassay (Pierce, Rockford, IL, USA). 1-Palmitoyl-2-oleoylphosphatidylcholine (POPC) and cholesterol (Chol) were purchased from Avanti Polar Lipids (Birmingham, AL, USA). The *N*-(5-dimethylaminonaphtalene-1-sulfonyl)-1,2-dihexadecanoyl-sn-glycero-3-phosphoethanolamine (d-DHPE), *N*-(7-nitro-benz-2-oxa-1,3-diazol-4-yl)phosphatidylethanolamine (N-NBD-PE), *N*-(lissamine rhodamine B sulfonyl)phosphatidylethanolamine (N-Rh-PE), and 6-dodecanoyl-2-dimethylaminonaphthalene (laurdan) fluorescent probes were from Molecular Probes (Eugene, OR, USA). Monoclonal antibody (MAb) 4E10 was a gift from Dietmar Katinger (Polymun Scientific, Klosterneuburg, Austria).

Fab expression and purification. Experimental procedures similar to those described in reference 27 were followed for the production and purification of Fab4E10 and its derived CDR-H3 ΔLoop mutant. The genes encoding Fab4E10 were synthesized (TOP Gene Technologies, Saint-Laurent, Quebec, Canada) and subsequently expressed from the pCOLADuet-1 vector (Novagen, Madrid, Spain). For generation of the Fab4E10-ΔLoop mutant, the hydrophobic CDR H3 loop apex (residues W_{100}-G_{100A}-W_{100B}-L_{100C}) was deleted through site-directed mutagenesis. The resulting gap between residues G_{99} and G_{100D} (ca. 6 Å) was filled with a SG dipeptide linker. 4E10 constructs were expressed in *Escherichia coli* T7 SHuffle strain (New England BioLabs, Barcelona, Spain). Bacterial cultures were induced at an optical density at 600 nm (OD_{600}) of 0.8 with 0.4 mM IPTG (isopropyl thiogalactopyranoside) and grown for 36 to 48 h at 16°C. Cells were harvested by centrifugation and resuspended in 50 mM HEPES (pH 7.5) and 500 mM NaCl supplemented with 5% glycerol, 35 mM imidazole, 1 mg/ml lysozyme, DNase, and an EDTA-free protease inhibitor mixture (Roche, Madrid Spain). Soluble Fabs were obtained by cell lysis using an Avestin Emulsiflex C5 homogenizer. Cell debris was removed by centrifugation, and the supernatant was loaded onto nickel-nitrilotriacetic acid (Ni-NTA) resin (GE Healthcare). Elution was performed with 500 mM imidazole, and the fractions containing His-tagged proteins were pooled, concentrated, and further purified using a HiLoad Superdex 75 prep-grade gel filtration column (GE Healthcare, Madrid, Spain). Purified protein was concentrated and stored at 4°C.

Lipid vesicle assays. Large unilamellar vesicles (LUV) were prepared following the extrusion method of Hope et al. (28). Phospholipids and cholesterol were mixed in chloroform and dried under a N_2 stream. Traces of organic solvent were removed by overnight vacuum pumping. Subsequently, the dried lipid films were dispersed in 5 mM HEPES and 100 mM NaCl (pH 7.4) buffer and subjected to 10 freeze-thaw cycles prior to extrusion 10 times through 2 stacked polycarbonate membranes (Nuclepore, Inc., Pleasanton, CA, USA). The size distributions of the vesicles were determined using a Malvern Zeta-Sizer Nano ZS instrument (Malvern Instruments, Malvern, United Kingdom). Extrusion through membranes with a nominal pore size of 0.1 μm produced POPC-Chol (1:1 [mol/mol]) LUV with mean diameters of ca. 120 nm. Phospholipid concentrations of liposome suspensions were determined by phosphate analysis. Chol content in vesicles was determined after extrusion by the cholesterol oxidase/peroxidase method (Biosystems, Barcelona, Spain) and found to be within the experimental error.

Membrane lipid mixing was monitored using the resonance energy transfer assay described by Struck et al. (29). The assay is based on the dilution of comixed N-NBD-PE and N-Rh-PE, whereby dilution due to membrane mixing results in increased N-NBD-PE fluorescence. In the classical format, vesicles containing 0.6 mol% of each probe were mixed with unlabeled vesicles at a ratio of 1:4 (final lipid concentration, 100 μM). The NBD emission was monitored at 530 nm with the excitation wavelength set at 465 nm. A cutoff filter at 515 nm was used between the sample and the emission monochromator to avoid scattering interference. The fluorescence scale was calibrated such that the zero level corresponded to the initial residual fluorescence of the labeled vesicles and the value of 100% corresponded to the complete mixing of all the lipids in the system. The latter value was set by the fluorescence intensity of vesicles labeled with 0.12 mol% of each fluorophore at the same total lipid concentration as in the fusion assay. Alternatively, fusion was assessed using peptide-activated vesicles committed for fusion. In this format, unlabeled vesicles (90 μM) were first incubated with peptide for 120 s and subsequently supplemented with fluorescently labeled vesicles (10 μM).

Determination of membrane rigidity was based on the estimation of the general polarization (GP) parameter using laurdan and multiphoton fluorescence microscopy of giant unilamellar vesicles (GUVs), as described in reference 30. Images of GUVs were acquired on a Leica TCS SP5 II microscope. For multiphoton excitation, the sample was illuminated with a 780-nm beam from a femtosecond-pulsed titanium-sapphire Mai Tai Deepsee laser (Spectra-Physics, Santa Clara, CA, USA). Fluorescent GUVs were imaged with a ×63 water immersion objective (numerical aperture [NA] = 1.2). Images were captured in 512- by 512-pixel format at a 400-Hz scan speed. The GP value for each pixel in the images was calculated using MATLAB (MathWorks, Natick, MA, USA)-based in-house-developed software and subsequently applied to obtain a GP value distribution for each individual vesicle. The mean GP value for each lipid mixture was calculated after imaging and processing of at least 30 GUVs.

Molecular dynamics simulations. Atomic coordinates of the HIV-1 gp41 MPER were taken from PDB entries 1JAV and 2PV6. Residues included in the model have the sequences NEQELLELDKWASLWNWF NITNWLWYIK (NpreTM) and NWFDITNWLWYIKLFIMIVGGLV (CpreTM). Default protonation states were used for all the ionizable residues. N and C termini were amidated and acetylated, respectively.

Pre-equilibrated model bilayers containing a mixture of POPC-Chol at ratios of 4:1 and 1:1 were used. The system was solvated by ~40.000 water molecules. Na^+ and Cl^- ions were added to neutralize the system up to a final experimental concentration of 150 mM. Either 4 or 12 peptides were randomly placed in the solution at the start of the simulation. The total production run was 720 ns.

MD trajectories were simulated with version 2.9 of NAMD (31), using the CHARMM force field with CMAP corrections (32) and using the TIP3P model for water molecules (33) and the model of Cournia et al. for Chol (34). Standard parameters for ions in the CHARMM force field were adopted. Simulations were performed in the NpT ensemble. Pressure was kept at 1 atm by the Nose-Hoover Langevin piston method (35, 36) with a damping time constant of 100 ps and a period of 200 ps. The temperature was kept at 300 K by coupling to a Langevin thermostat, with a damping coefficient of 5 ps^{-1} (36). Electrostatic interactions were treated by the particle mesh Ewald algorithm, with grid spacing below 1 Å (37). Van der Waals interactions were truncated at 12 Å and smoothed at 10 Å. Hydrogen atoms were restrained by the SETTLE algorithm (38), which allowed a 2-fs time step.

Atomic force microscopy. Atomic force microscopy (AFM) measurements were performed on bilayers supported on a mica substrate. Supported planar bilayers (SPBs) were left to equilibrate at room temperature for 30 min before AFM measurements were taken. Peptide-containing samples were further incubated for 30 min before data acquisition. The measurements were performed on a NanoWizard II AFM (JPK Instruments, Berlin, Germany) at 25°C. MLCT SiN cantilevers (Veeco Instruments, Plainview, NY, USA) with a spring constant of 0.1 N/m were used in contact or tapping mode scanning to measure the SPBs. Resolution images measuring 512 by 512 pixels were collected at a scanning rate between 1 and 1.5 Hz and line fitted using JPK image processing software as required.

Cell entry assays. For the neutralization assays (27), HIV-1 pseudoviruses were produced by transfection of human kidney HEK293T cells with the full-length Env clone JRCSF (kindly provided by Jamie K. Scott and Naveed Gulzar, Simon Fraser University, Burnaby, BC, Canada) using calcium phosphate. Cells were cotransfected with vectors pWXLP-GFP and pCMV8.91, encoding a green fluorescent protein and an *env*-deficient HIV-1 genome, respectively (provided by Patricia Villace, CSIC, Madrid, Spain). After 24 h, the medium was replaced with Optimem-Glutamax II (Invitrogen Ltd., Paisley, United Kingdom) without serum. Two days after transfection, the pseudovirus particles were harvested, passed through 0.45-μm-pore sterile filters (Millex HV; Millipore NV, Brussels, Belgium), and finally concentrated by ultracentrifugation in a sucrose gradient. HIV entry was determined using TZM-bl target cells (AIDS Research and Reference Reagent Program, Division of AIDS, NIAID, NIH; contributed by J. Kappes). Antibody samples were set up in duplicate in 96-well plates and incubated for 1.5 h at 37°C with a 10 to 15% tissue culture infectious dose of pseudovirus. After antibody-pseudovirus coincubation, 11,000 target cells were added in the presence of 30 μg/ml DEAE-dextran (Sigma-Aldrich, St-Louis, MO). Infection levels after 72 h were inferred from the number of green fluorescent protein (GFP)-positive cells as determined by flow cytometry using a BD FACSCalibur flow cytometer (Becton Dickinson Immunocytometry Systems, Mountain View, CA).

RESULTS

Figure 1A schematically displays the prevailing model for Env-mediated cell-virus membrane fusion. In line with previous sequence-based predictions (16, 39), recent structural studies support that the gp41 region in contact with viral lipids may span the TMD plus the adjacent MPER sequence in the native prefusion state (9, 10). In this study, we have designed three overlapping peptides spanning the complete MPER-TMD region (Env residues 656 to 704) (Fig. 1B). The sequence range covered by each of these peptides was selected on the basis of the conserved hydrophobicity profiles and the presence of hinges delimiting helical subdomains. In brief, the aromatic-rich NpreTM peptide derives from the canonical MPER sequence that precedes the predicted TMD. Regarding hydrophobicity, this peptide combines two conserved interfacial helices jointed by the ^{671}NWFD^{674} hinge (40, 41). CpreTM covers the C-terminal MPER block and the N-terminal hydrophobic section of the TMD preceding a putative kink at Gly-692 (39, 42). Finally, the sequence of TMDp was defined according to previous functional studies by Cohen and coworkers (43).

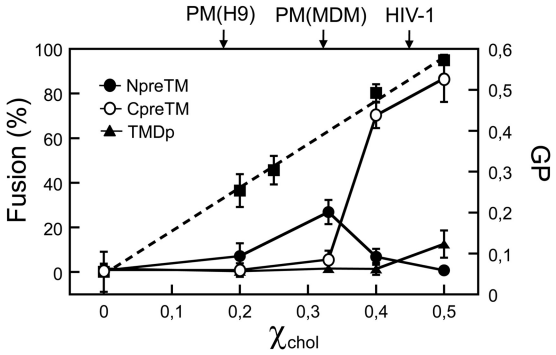

FIG 2 Fusion activity of MPER-TMD peptides as a function of membrane rigidity. Levels of fusion (lipid-mixing assay) measured after a 10-min incubation with NpreTM, CpreTM, or TMDp were plotted against the Chol mole fraction. The peptide-to-lipid molar ratio was 1:25 in all cases. Plotted values are means ± standard deviations (SD) from three experiments. Membrane order (dotted line and squares) ranged from GP values of 0.05 (most fluid) to 0.6 (most rigid), as measured in GUVs. Arrows on top mark Chol contents in the plasma membrane of virus-producing H9 and MDM cells (26) and virions (24).

To determine the capacity of MPER-TMD-derived sequences for fusing rigid membranes, we compared the lipid-mixing activity displayed by NpreTM, CpreTM, and TMDp as a function of the Chol content (Fig. 2 and 3). Figure 2 correlates the membrane order increase ensuing upon Chol addition with peptide-induced fusion. Membrane ordering was monitored by two-photon microscopy of laurdan-labeled giant unilamellar vesicles as described previously (30). Consistent with the increase in rigidity, the general polarization order parameter increased linearly with the Chol content (Fig. 2, squares). Order increase had a significant effect on CpreTM activity (Fig. 2, open circles). Fusion induced by this peptide reached almost 100% in the most rigid vesicles but decreased sharply upon fluidification and was totally inhibited with Chol concentrations lower than 30 mol%. In contrast, the MPER section represented by the NpreTM peptide displayed a bimodal behavior (Fig. 2, filled circles). Consistent with previously reported results (44), certain degree of fusion activity could be observed for POPC-Chol 2:1 vesicles, but the effect was inhibited with higher or lower Chol concentrations. Marginal fusion was also observed for TMDp, restricted in this case to the high Chol concentration range (Fig. 2, triangles). Overall, these data pinpoint the region covered by CpreTM as a fusogen of rigid membranes which loses activity upon their fluidification. Of note, the fusion induced by CpreTM occurred at Chol concentrations comparable to those existing at the viral envelope (24), while the peptide remained fusion inactive at the concentrations described to occur at the plasma membrane of the producer cells (26). The preceding or following sequences, which only included portions of CpreTM, were barely fusogenic under the same conditions.

To study the peptide dose dependency, fusion was assessed using vesicles containing 50 mol% Chol (Fig. 3). Again, significant induction of vesicle fusion was observed only for the section covered by CpreTM (Fig. 3, middle). The measured EC_{50} corresponded to peptide-to-lipid ratios of around 1:250 (mol/mol). These low membrane doses further suggest that fusion did not evolve as a consequence of hydrophobic adsorption of massive amounts of peptide to the lipid bilayer but rather as a result of an intrinsic membrane activity of the CpreTM sequence.

To get insights into the molecular mechanism of the Chol-dependent membrane fusion, CpreTM effects were subsequently characterized by combining MDS and AFM methods (Fig. 4 and 5). According to the MDS, when 4 peptides were added to POPC-Chol (1:1) bilayers, the CpreTM sequence induced disruption of the interface (Fig. 4A, left). Detailed views of these perturbing effects revealed promotion of phospholipid protrusion and acyl chain exposure (Fig. 4A, right). Moreover, these disruptive effects were enhanced upon increasing the number of CpreTM mono-

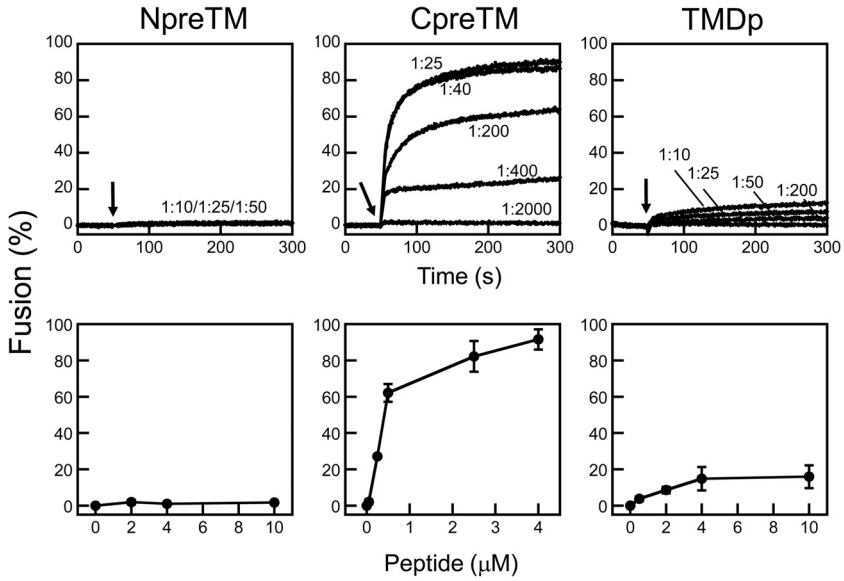

FIG 3 Fusion of POPC-Chol (1:1 molar ratio) vesicles induced by NpreTM, CpreTM, and TMDp peptides. (Top) Kinetics of fusion (lipid-mixing assay). Peptides were added to vesicle suspensions at the indicated peptide-to-lipid ratios. The time of addition was 50 s (arrow). The lipid concentration was 100 μM. (Bottom) Final extents of fusion. The percentage of lipid-mixing measured after a 10 min incubation of peptides with vesicles has been plotted as a function of the peptide concentration. Values are means ± SD from three different experiments.

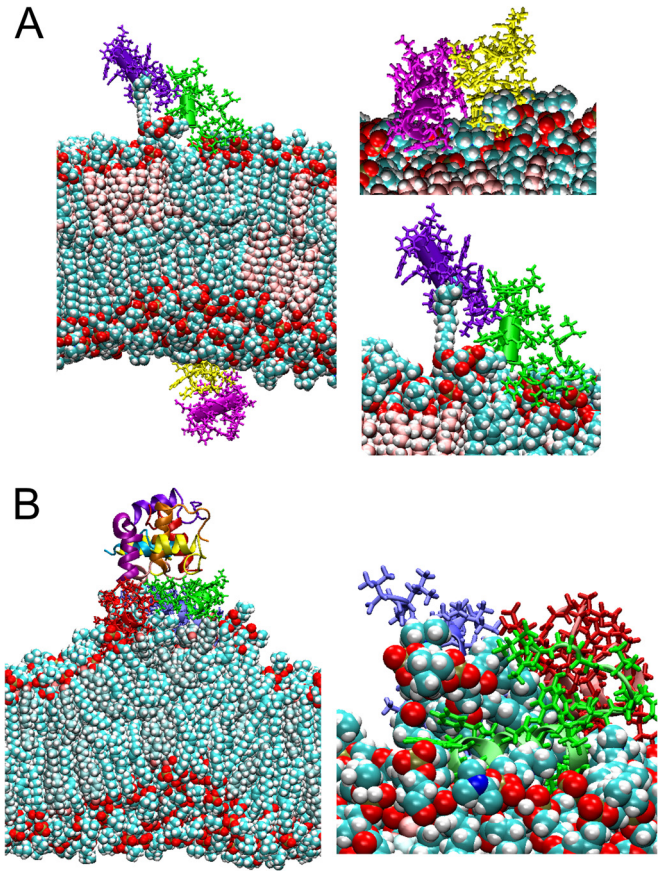

FIG 4 MDS of CpreTM sequence interacting with POPC-Chol (1:1 molar ratio) lipid bilayers. (A) The simulation considered 4 peptides. The snapshot was taken at 112 ns. Peptides are displayed in stick-and-ribbon format, and phospholipids and Chol are shown in a space-filling representation. Close views in the right panels illustrate polar-head group engagement (top) and acyl-chain splaying (bottom). (B) The simulation considered 12 peptides. (Left) Snapshot of CpreTM-induced disruption of POPC-Chol (1:1) bilayers (taken at 360 ns). (Right) Close view illustrating the phospholipid extraction phenomenon.

mers considered in the simulation (Fig. 4B). In those instances, higher-order aggregates inserted into the bilayer seemed to cooperate to extract lipids, the process evolving in a focal point with negative monolayer curvature (Fig. 4B, left). These interactions eventually resulted in the complete extraction and exposure to solvent of phospholipid molecules, including their acyl chain moieties (Fig. 4B, right).

To experimentally determine the effects of the disruptive interactions unveiled by the MDS (Fig. 5A), supported membranes were treated with CpreTM and studied by AFM. Figure 5B compares visual fields of untreated and CpreTM-treated POPC-Chol (1:1) SPBs. The average height of the untreated control samples (Fig. 5B, left) was consistent with the formation of lipid bilayers in our system (data not shown). These samples displayed a homogeneous surface. In contrast, incubation of these bilayers with 0.01 μM peptide caused the formation of randomly distributed fissures with comparable sizes (Fig. 5B, center). The depth of these cavities relative to the surface of the bilayer was estimated in the range of 3 to 4 nm, while their brinks regularly displayed greater height differences. Increasing the amount of peptide (0.1 μM) resulted in heavily perforated lipid bilayers displaying more accumulation of material at the edges of the lesions (Fig. 5B, right). Thus, according to the AFM observations, the CpreTM peptide generated membrane lesions in the bilayer that were compatible with phospholipid extraction and its accumulation on the surface.

The data displayed in Fig. 5C further show that these membrane-disruptive effects were not reproduced by the NpreTM sequence inserted into the membrane interface of the POPC-Chol (1:1) bilayer (Fig. 5C, top), nor by CpreTM interacting with lipid bilayers containing smaller amounts of Chol (i.e., POPC-Chol [4:1]) (Fig. 5C, bottom). The MDS snapshots displayed on the left revealed in those instances interactions with membrane surfaces not leading to phospholipid extraction or acyl chain exposure during the recorded time. Consistently, AFM examination revealed rounded spots with a slight decrease in depth (ca. 1 nm) in POPC-Chol (1:1) SPBs treated with NpreTM, while CpreTM did not perturb so intensely the architecture of the POPC-Chol (4:1) SPBs (Fig. 5C, right).

Overall, results displayed in Fig. 2 to 5 support a functional role for the CpreTM sequence as a supplementary FP, which would be active in the context of Chol-enriched rigid membranes by extracting phospholipids at the fusion loci. Data displayed in Fig. 6 and 7 further suggest that such membrane activity could represent the target for broadly neutralizing anti-MPER antibodies such as 4E10. The MDS data displayed in Fig. 6A (left) disclosed the 4E10 epitope region exposed to solvent when CpreTM is anchored to POPC-Chol (1:1) bilayers. Docking of the 4E10 Fab structure further supported accessibility for antibody binding (Fig. 6A, right). Remarkably, after docking, the Fab positioned the paratope surface in contact with the membrane surface, while the CDR-H3 loop tip required for neutralization was inserted shallowly into the bilayer interface, as previously predicted (45).

To experimentally determine 4E10's capacity for binding the membrane-inserted CpreTM functional form, we assessed the activity of this antibody in a committed-fusion assay (Fig. 6B). Thus, the previous MDS suggest that CpreTM-induced perturbations may prime the Chol-enriched membrane for fusion. To test that possibility, we set up a committed-fusion experimental condition under which vesicles were first activated by CpreTM addition. At the outset, we ensured that under the conditions selected for priming the membranes, the amount of peptide remaining unbound in solution was negligible (data not shown). Further coincubation of the activated vesicles with fluorescently labeled target vesicles resulted in membrane fusion, monitored as the dilution of the probes into the whole vesicle population (Fig. 6B, black traces).

Consistent with binding to the fusogenic form of CpreTM, addition of MAb4E10 to "peptide-activated" vesicles halted fusion (Fig. 6B, left). The inhibitory effect was not observed when vesicles were fusion activated with the Cala peptide, which bears the 4E10 epitope key dipeptide ^{672}WF^{673} mutated to Ala residues (46) (Fig. 6B, right). Together, these results demonstrate that the capacity of 4E10 antibody for inhibiting the committed fusion process was a dose- and epitope recognition-dependent phenomenon.

The physiological relevance of this fusion inhibition phenomenon was further inferred from the results displayed in Fig. 7. In those experiments, we compared the Fab4E10-WT with its Fab4E10-ΔLoop variant, the latter having the hydrophobic CDR-H3 loop tip deleted (Fig. 7, left and right, respectively). The WT and ΔLoop Fabs disclosed comparable secondary structures

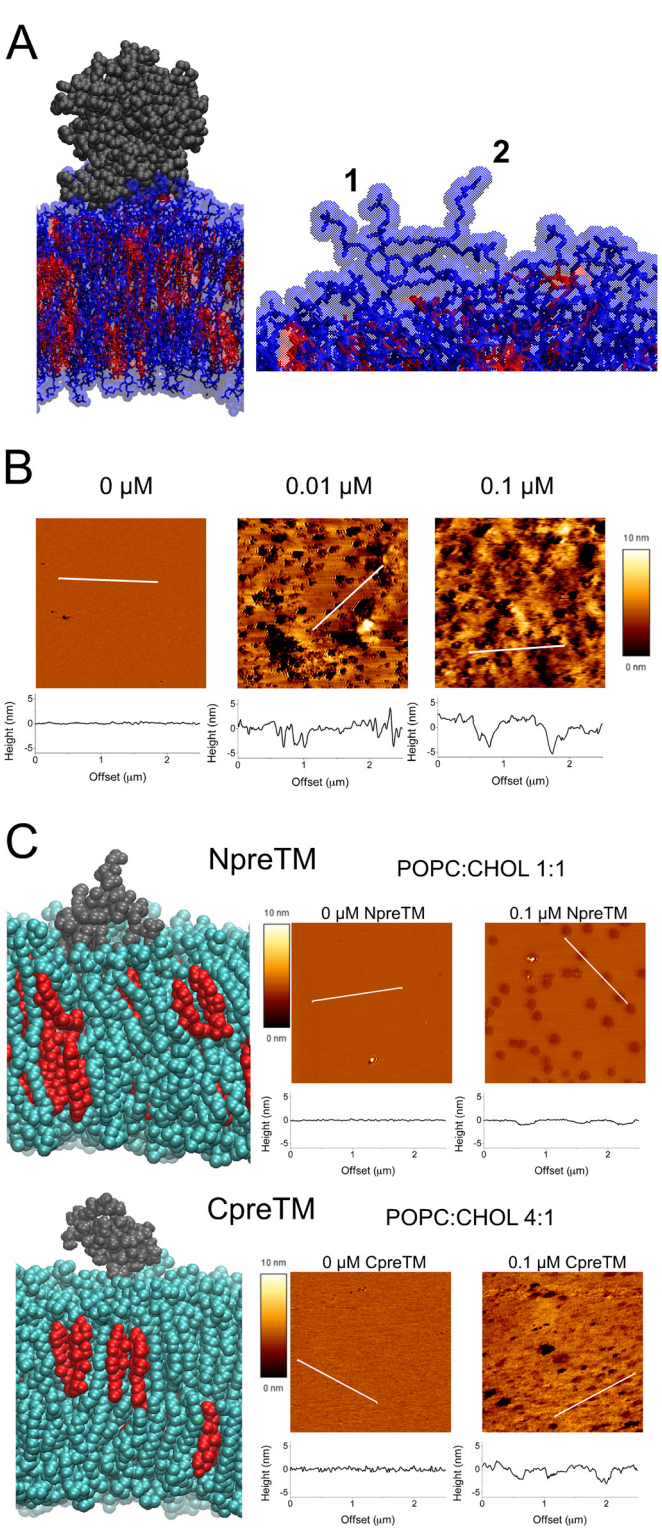

FIG 5 Structural alterations of lipid bilayers. (A) MDS of membrane surface alteration by CpreTM. (Left) Snapshot of CpreTM interacting with POPC-Chol (1:1) lipid bilayers. The peptides are displayed in space-filling representation (gray), and phospholipids and Chol are shown in semitransparent molecular surface-and-stick representation (blue and red, respectively). (Right) Phospholipid head group protrusions (1) and acyl-chain exposure (2) when the peptide is omitted. (B) AFM height images of POPC-Chol (1:1) SPBs. An untreated control sample (left) is compared with SPBs that were treated with 0.01 and 0.1 μM CpreTM (center and right, respectively). Images of CpreTM-containing samples were obtained 30 min after peptide addition. Sizes of visual fields are 4.5 by 4.5 μm. Plots below the images display the height profiles for the trajectories indicated by the white lines. (C) Interactions of NpreTM (top) and CpreTM (bottom) with POPC-Chol (1:1) and POPC-Chol (4:1) membranes, respectively. (Left) MDS snapshots taken at 100 ns. Peptides (gray) and lipids (POPC, green; Chol, red) are displayed in space-filling representation. (Right) AFM height images (conditions were as described for panel B).

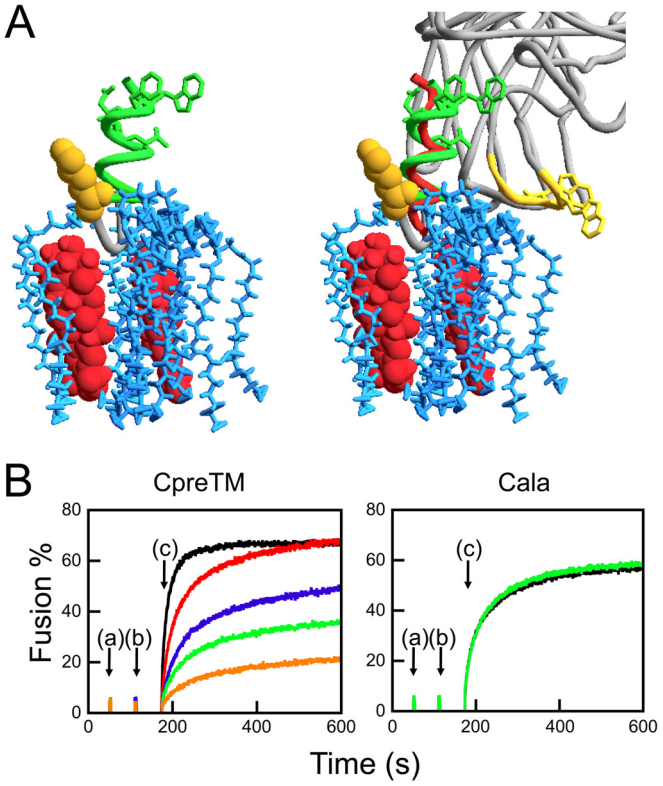

FIG 6 Fusion inhibition by 4E10 MAb. (A) (Left) Accessibility of the 4E10/10E8 epitope region (in green) on the membrane surface according to MDS of CpreTM interacting with POPC-Chol (1:1) bilayers. Side chain of Lys-683 is displayed in orange. Phospholipids (stick representation) and Chol (space-filling representation) are in blue and red, respectively. The snapshot was taken at 100 ns. (Right) Docking of the 4E10 paratope into the previous structure. To create the figure, the peptide bound to Fab4E10 in the crystal structure with PDB code 2FX7 was fitted into the simulated CpreTM peptide. The CDR-H3 loop and the side chains of Trp residues within are highlighted in yellow. (B) (Left) Vesicles were primed for fusion with CpreTM (a), and after 60 s (b), they were treated with 1 (red), 2 (blue), 5 (green), or 10 (orange) μg/ml of MAb4E10. The black trace corresponds to the control in the absence of antibody. Finally, the mixture was supplemented with fluorescently labeled vesicles, and the remaining fusion activity was monitored over time (c). (Right) Vesicles were primed with Cala peptide, and the MAb effect was assessed under the same conditions.

(Fig. 7A) and binding to soluble peptide epitope (Fig. 7B), thereby confirming that the generated mutation did not interfere with the overall structure or stability of the 4E10 binding fragment. In contrast, the ΔLoop mutation did interfere with the ability of this Fab to block pseudovirus infection (Fig. 7C) and to inhibit liposome fusion (Fig. 7D). Thus, cell entry blocking and fusion inhibition phenomena seem to depend on the correct sequence of the 4E10 CDR-H3 loop.

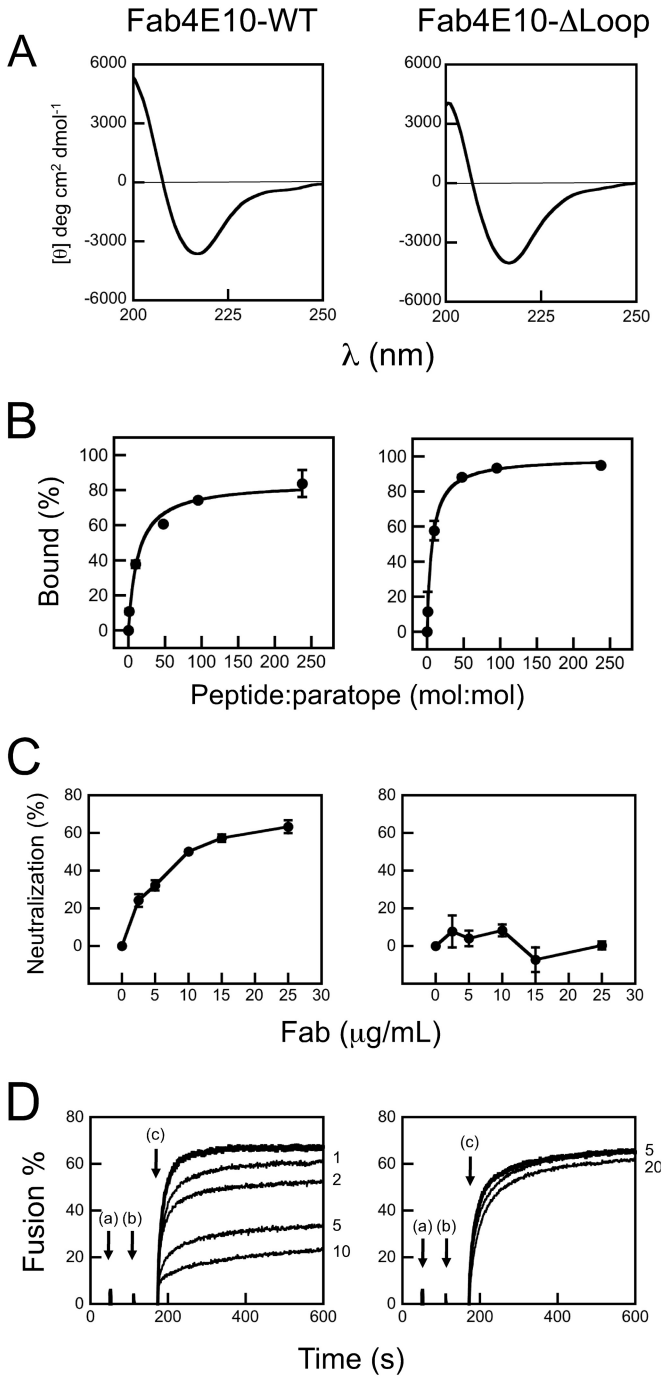

FIG 7 Comparison of the 4E10 Fab (left) and its derived ΔLoop mutant (right). (A) Circular dichroism spectra of Fab4E10-WT and Fab Fab4E10-ΔLoop mutant. Negative absorption at 217 nm observed in both cases was consistent with adoption of a main β-structure. (B) Binding to the soluble peptide epitope. Competitive enzyme-linked immunosorbent assays (ELISAs) were performed using plates coated with CpreTM (1.4 μM). Prior to being added to the plates, Fabs were preincubated for 30 min with serial dilutions of soluble peptide-epitope (NWFDITNWLWYIK-*KKK*). Percentages of binding inhibition were determined in duplicate and adjusted to saturation curves. (C) Cell entry inhibition assay. Pseudoviruses were preincubated with Fab, and single cell entry events were monitored by fluorescence-activated cell sorting (FACS) after incubation with TZM-bl target cells. Means ± SD of 4 measurements from 2 independent experiments are displayed. (D) Fusion inhibition. (Left) Vesicles were primed for fusion with CpreTM (a), and after 60 s (b) they were treated with 1, 2, 5, or 10 μg/ml of Fab4E10-WT, as indicated. The thicker trace on top corresponds to the control in the absence of antibody. (Right) At the time indicated by the arrow (b), vesicles were supplemented with 5 or 20 μg/ml of Fab4E10-ΔLoop, as indicated. Conditions are otherwise as described for Fig. 6.

DISCUSSION

The exaggerated rigidity of the viral envelope poses a challenge to the description of the HIV fusion mechanism according to current paradigms of lipid bilayer remodeling (11, 15, 47). The proposed fusion models are based on a continuous approach of membranes in terms of their elastic properties and establish that inserted FP moieties may promote lipid bilayer disruption and/or deformation along the fusion pathway. Thus, according to this view, the FPs may locally dehydrate the membrane interface, generate hydrophobic patches, impart curvature, and/or soften the lipid bilayer to catalyze membrane merger (see reference 14 for a recent review on this matter).

It has been hypothesized that gp41's ability for restructuring the viral membrane resides within the MPER sequence (16, 18, 19, 48). Some authors propose that hydrophobic insertion of the FP and MPER domains into cell and viral membranes, respectively, might generate the bulging out of the approaching bilayers during HIV fusion (11, 17, 48). The bent lipid bilayer at the end cap of each bulge would be fusion prone because its curvature and the associated elastic energy would relax in the course of the fusion reaction (11). A flaw in this fusion model is that the strong lipid cohesion induced by the high Chol content of the viral membrane (in the range of 40 to 50 mol% [24, 26, 49]) is predicted first to act against the opening of cavities required for transferring MPER residues into the membrane (50) and then to alter the bilayer mechanical properties, including the area compressibility modulus (51), the bending modulus (52), and the spontaneous radius of curvature (53), to oppose fusion-related deformations evolving thereafter (15).

Counterintuitively, it has been argued that the high Chol content of the viral envelope constitutes a structural component of the virion required for the cell entry function. This idea is supported by observations indicating that interference with (54, 55) or depletion of (56–58) this compound abolishes HIV infectivity. In particular, early fluidity measurements by Aloia et al. (25) indicated that the Chol-enriched HIV-1 envelope is among the most rigid membranes and that its fluidification may reduce infectivity. It is tempting to speculate that Chol itself may take part in the fusion reaction, either by directly interacting with MPER, as suggested by some authors (59), or as a cofactor (18, 60).

The MPER-TMD region appears to be composed of an articulated helix that is particularly enriched in conserved aromatic residues at the junction between both domains (Fig. 1B). In this work, we approached the MPER-TMD function using overlapping peptides. In addition, a two-lipid model system was selected to specifically modulate membrane rigidity as a function of the Chol content. Although the selected POPC-Chol vesicles allowed monitoring of changes on the membrane activity of the peptides as a function of a single factor, both experimentally (Fig. 2, 3, and 5) and *in silico* (Fig. 4 and 5), we caution that this simple model is devoid of the compositional complexity found in cell membranes (61).

From the comparison of the fusion capacities displayed by the overlapping peptides as a function of membrane rigidity (Fig. 2), it

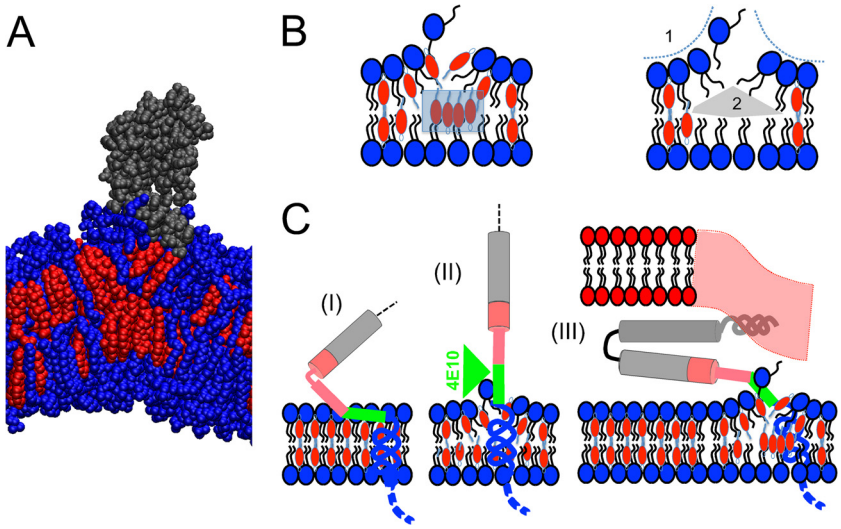

FIG 8 Proposed activity for the gp41 sequence covered by CpreTM peptide during HIV membrane fusion. (A) MDS snapshot displaying phospholipid extraction from the interface and Chol stacking in the opposing monolayer. (B) (Left) Cartoon representation of lipids displayed in panel A. (Right) Chol molecules have been omitted to highlight their possible effects on the phospholipid matrix. Chol may help promote phospholipid extraction by stabilizing negative curvature of the monolayer (1) and/or by filling interlamellar voids (2). (C) Functioning of the section covered by the CpreTM sequence in the context of Env-mediated fusion. (Left) In the prefusion state (I in Fig. 1A), the CpreTM region may be concealed at the base of the ectodomain and inserted parallel to the membrane plane. (Center) Possible role in a prehairpin configuration (state II in Fig. 1A). Orienting conserved aromatic residues at the MPER-TMD junction perpendicular to the membrane plane may promote phospholipid extraction. The model supports the possibility of 4E10 binding to lipids concomitantly to the protein epitope. (Right) Closure of the hairpin might couple disruption of the viral membrane to fusion. Phospholipid molecules whose acyl chains are splayed may establish a lipid connection between contacting bilayers. The ectodomain is proposed to bend again at the ^{671}NWFD^{674} elbow in this state.

can be inferred that the CpreTM spanning gp41 sequence might embody a C-terminal FP capable of fusing rigid membranes enriched in cholesterol. In comparison, the NpreTM peptide, which derived from the MPER section previously assumed to represent a membrane-perturbing domain (16, 18, 19, 60), showed no activity under those conditions (Fig. 3). Surprisingly, reduction of the Chol content and membrane order correlated with a loss of CpreTM's fusogenic activity.

MDS provided unprecedented insights at the molecular level, on the mechanism underlying the CpreTM-induced, Chol-dependent fusion phenomenon (Fig. 4 and 5). In simulations of POPC-Chol (1:1) lipid bilayers, CpreTM was found to extract individual phospholipid molecules and expose them to solvent. The membrane perturbations ensuing after these interactions were experimentally characterized by *in situ* AFM of SPBs (Fig. 5B and C). CpreTM generated membrane lesions consistent with the capacity of the gp41 MPER-TMD junction for extracting phospholipid from the viral lipid bilayer during the HIV fusion process.

Thus, we infer that the initial states of the CpreTM-induced fusion process might be reminiscent of the lipid tail protrusion mechanism formulated by Kinnunen and Holopainen (62), also proposed to underlie fusion induced by the influenza virus FP interacting with membranes (63). In brief, Kinnunen and Holopainen postulate that packing strain arising from negative curvature can be relieved by the adoption of an extended conformation by phospholipids (62, 64). In that conformation, one of the acyl chains would stick out into the aqueous phase. It has been reasoned that a lipid molecule whose two acyl chains are splayed may suffice to build an initial lipid bridge between contacting bilayers, a process eventually leading to the mixing of the constituent lipids (47). By analogy, the negative curvature arising from interactions of polar-head groups with aromatic residues located within CpreTM external to the bilayer plane might eventually provoke acyl chain extraction (Fig. 8).

An inspection of the snapshot displayed in Fig. 8A provides insights into the Chol requirement for CpreTM activity. The explanatory cartoon displayed in Fig. 8B illustrates two possible contributions of Chol to the fusion process. First, this compound seems to buttress the negative monolayer curvature generated in the proximity of the peptide (Fig. 8B, dotted lines). Second, Chol molecules appear to fill the void arising in between the opposing monolayers during the process. Filling this void by several stacking Chol molecules is likely required to stabilize the curved state of the opposing monolayer. Upon depletion of Chol, formation of these clusters could not be observed in the simulations, while CpreTM insertion did not result in membrane interface disruption (Fig. 5C). We conclude that Chol can be recruited to promote and stabilize focal points of negative curvature, which in turn may assist CpreTM catalyze acyl-chain protrusion.

According to this model, the fusogenic activity of CpreTM was probably due to the positioning of aromatic residues close to but external to the membrane interface. The disruptive capacity is likely intensified for peptides that are inserted perpendicular to the lipid bilayer plane, an arrangement further assisted by self-oligomerization at the membrane surface. In contrast, NpreTM did not reproduce the lipid protrusion activity. One possibility that might explain this differential effect is that NpreTM inserted into POPC-Chol (1:1) bilayers mostly oriented with the main helix parallel to the membrane plane. In this orientation, aromatics were stably embedded into the membrane interface without inducing a negative monolayer curvature, as has been previously demonstrated for a slightly shorter peptide (65).

Figure 8C compiles all these possibilities into a general model

for Env-mediated virus-cell membrane fusion. In the prefusion state (I), MPER might be concealed at the bottom of the glycoprotein complex by interacting with the viral membrane mostly oriented parallel to the bilayer plane. In the prehairpin intermediate (II), self-oligomerization of the CpreTM section might ensue, thereby relocating aromatic residues in close proximity but external to the membrane interface. In this state, phospholipid extraction would be favored. Upon 6-HB formation (III), the viral membrane focally disrupted at the MPER-TMD junction would be pulled into contact with the cell membrane. Phospholipid molecules whose acyl chains are splayed might prime the rigid envelope for merger.

It has been argued that HIV-1 may enter target cells through endocytosis and fusion with endosomes (66, 67). According to this line of evidence, viral particles may exchange lipids with the plasma membrane, while occurrence of the release of their luminal content is mainly restricted to intracellular compartments that are not connected to the plasma membrane. Thus, plasma membrane-virus fusion would be arrested at a hemifusion stage, while progression to fusion pore formation and dilation would require assistance by endosome-resident factors. According to such a mechanism, the lipid protrusion activity of the MPER-TMD connection would evolve in the context of the cell surface and would therefore be accessible to blocking factors from the external medium (68). The observation that the functional 4E10 antibody could halt the CpreTM-induced fusion process would be compatible with this possibility (Fig. 6, 7).

Finally, our findings may have implications for understanding the origin of the broad neutralization by antibodies binding to the MPER C terminus. Within the framework of the lipid protrusion model, maintenance of conserved aromatic residues and helical conformation at the C-terminal side of MPER seem to be a functional prerequisite. 4E10 antibody recognizes such a motif and seems to target the fusion intermediate of gp41 (69). As put forward by the model displayed in Fig. 8C (center), the aromatic-rich CpreTM section protruding orthogonally from the bilayer in the prehairpin state (Fig. 1A, step II) could, in association, bear extracted phospholipid. Thus, it is tempting to speculate that 4E10 might bind tightly to a proteolipid epitope and further arrest the fusion process. The existence of such a proteolipid binding mechanism might help reconcile contradictory reports on the capacity of anti-MPER antibodies for direct binding to membrane phospholipids (44, 69–74).

ACKNOWLEDGMENTS

We acknowledge financial support from the Spanish MINECO (BIO2011-29792), the Basque Government (IT838-13), and the National Institutes of Health (Bethesda, MD, USA) (1R01AI097051-01).

C. Domene acknowledges the use of computational resources from the EPSRC UK National Service for Computational Chemistry Software (NSCCS), the Hartree Center, the Red Española de Supercomputación, and Temple University (Philadelphia, PA, USA).

REFERENCES

1. **Eckert DM, Kim PS.** 2001. Mechanisms of viral membrane fusion and its inhibition. Annu. Rev. Biochem. **70:**777–810. http://dx.doi.org/10.1146/annurev.biochem.70.1.777.
2. **Gallo SA, Finnegan CM, Viard M, Raviv Y, Dimitrov A, Rawat SS, Puri A, Durell S, Blumenthal R.** 2003. The HIV Env-mediated fusion reaction. Biochim. Biophys. Acta **1614:**36–50. http://dx.doi.org/10.1016/S0005-2736(03)00161-5.
3. **Melikyan GB.** 2008. Common principles and intermediates of viral protein-mediated fusion: the HIV-1 paradigm. Retrovirology **5:**111. http://dx.doi.org/10.1186/1742-4690-5-111.
4. **Wyatt R, Sodroski J.** 1998. The HIV-1 envelope glycoproteins: fusogens, antigens, and immunogens. Science **280:**1884–1888. http://dx.doi.org/10.1126/science.280.5371.1884.
5. **Roux KH, Taylor KA.** 2007. AIDS virus envelope spike structure. Curr. Opin. Struct. Biol. **17:**244–252. http://dx.doi.org/10.1016/j.sbi.2007.03.008.
6. **Julien JP, Cupo A, Sok D, Stanfield RL, Lyumkis D, Deller MC, Klasse PJ, Burton DR, Sanders RW, Moore JP, Ward AB, Wilson IA.** 2013. Crystal structure of a soluble cleaved HIV-1 envelope trimer. Science **342:**1477–1483. http://dx.doi.org/10.1126/science.1245625.
7. **Lyumkis D, Julien JP, de Val N, Cupo A, Potter CS, Klasse PJ, Burton DR, Sanders RW, Moore JP, Carragher B, Wilson IA, Ward AB.** 2013. Cryo-EM structure of a fully glycosylated soluble cleaved HIV-1 envelope trimer. Science **342:**1484–1490. http://dx.doi.org/10.1126/science.1245627.
8. **Bartesaghi A, Merk A, Borgnia MJ, Milne JL, Subramaniam S.** 2013. Prefusion structure of trimeric HIV-1 envelope glycoprotein determined by cryo-electron microscopy. Nat. Struct. Mol. Biol. **20:**1352–1357. http://dx.doi.org/10.1038/nsmb.2711.
9. **Klasse PJ, Depetris RS, Pejchal R, Julien JP, Khayat R, Lee JH, Marozsan AJ, Cupo A, Cocco N, Korzun J, Yasmeen A, Ward AB, Wilson IA, Sanders RW, Moore JP.** 2013. Influences on trimerization and aggregation of soluble, cleaved HIV-1 SOSIP envelope glycoprotein. J. Virol. **87:**9873–9885. http://dx.doi.org/10.1128/JVI.01226-13.
10. **Khayat R, Lee JH, Julien JP, Cupo A, Klasse PJ, Sanders RW, Moore JP, Wilson IA, Ward AB.** 2013. Structural characterization of cleaved, soluble HIV-1 envelope glycoprotein trimers. J. Virol. **87:**9865–9872. http://dx.doi.org/10.1128/JVI.01222-13.
11. **Kozlov MM, McMahon HT, Chernomordik LV.** 2010. Protein-driven membrane stresses in fusion and fission. Trends Biochem. Sci. **35:**699–706. http://dx.doi.org/10.1016/j.tibs.2010.06.003.
12. **Blumenthal R, Durell S, Viard M.** 2012. HIV entry and envelope glycoprotein-mediated fusion. J. Biol. Chem. **287:**40841–40849. http://dx.doi.org/10.1074/jbc.R112.406272.
13. **Melikyan GB.** 2011. Membrane fusion mediated by human immunodeficiency virus envelope glycoprotein. Curr. Top. Membranes **68:**81–106. http://dx.doi.org/10.1016/B978-0-12-385891-7.00004-0.
14. **Apellaniz B, Huarte N, Largo E, Nieva JL.** 2014. The three lives of viral fusion peptides. Chem. Phys. Lipids **181C:**40–55. http://dx.doi.org/10.1016/j.chemphyslip.2014.03.003.
15. **Chernomordik LV, Kozlov MM.** 2003. Protein-lipid interplay in fusion and fission of biological membranes. Annu. Rev. Biochem. **72:**175–207. http://dx.doi.org/10.1146/annurev.biochem.72.121801.161504.
16. **Suarez T, Gallaher WR, Agirre A, Goni FM, Nieva JL.** 2000. Membrane interface-interacting sequences within the ectodomain of the human immunodeficiency virus type 1 envelope glycoprotein: putative role during viral fusion. J. Virol. **74:**8038–8047. http://dx.doi.org/10.1128/JVI.74.17.8038-8047.2000.
17. **Buzon V, Natrajan G, Schibli D, Campelo F, Kozlov MM, Weissenhorn W.** 2010. Crystal structure of HIV-1 gp41 including both fusion peptide and membrane proximal external regions. PLoS Pathog. **6:**e1000880. http://dx.doi.org/10.1371/journal.ppat.1000880.
18. **Shnaper S, Sackett K, Gallo SA, Blumenthal R, Shai Y.** 2004. The C- and the N-terminal regions of glycoprotein 41 ectodomain fuse membranes enriched and not enriched with cholesterol, respectively. J. Biol. Chem. **279:**18526–18534. http://dx.doi.org/10.1074/jbc.M304950200.
19. **Vishwanathan SA, Hunter E.** 2008. Importance of the membrane-perturbing properties of the membrane-proximal external region of human immunodeficiency virus type 1 gp41 to viral fusion. J. Virol. **82:**5118–5126. http://dx.doi.org/10.1128/JVI.00305-08.
20. **Kwong PD, Mascola JR.** 2012. Human antibodies that neutralize HIV-1: identification, structures, and B cell ontogenies. Immunity **37:**412–425. http://dx.doi.org/10.1016/j.immuni.2012.08.012.
21. **Klein F, Mouquet H, Dosenovic P, Scheid JF, Scharf L, Nussenzweig MC.** 2013. Antibodies in HIV-1 vaccine development and therapy. Science **341:**1199–1204. http://dx.doi.org/10.1126/science.1241144.
22. **Huang J, Ofek G, Laub L, Louder MK, Doria-Rose NA, Longo NS, Imamichi H, Bailer RT, Chakrabarti B, Sharma SK, Alam SM, Wang T, Yang Y, Zhang B, Migueles SA, Wyatt R, Haynes BF, Kwong PD, Mascola JR, Connors M.** 2012. Broad and potent neutralization of HIV-1

by a gp41-specific human antibody. Nature **491:**406–412. http://dx.doi.org/10.1038/nature11544.
23. **Binley JM, Wrin T, Korber B, Zwick MB, Wang M, Chappey C, Stiegler G, Kunert R, Zolla-Pazner S, Katinger H, Petropoulos CJ, Burton DR.** 2004. Comprehensive cross-clade neutralization analysis of a panel of anti-human immunodeficiency virus type 1 monoclonal antibodies. J. Virol. **78:**13232–13252. http://dx.doi.org/10.1128/JVI.78.23.13232-13252.2004.
24. **Brugger B, Glass B, Haberkant P, Leibrecht I, Wieland FT, Krausslich HG.** 2006. The HIV lipidome: a raft with an unusual composition. Proc. Natl. Acad. Sci. U. S. A. **103:**2641–2646. http://dx.doi.org/10.1073/pnas.0511136103.
25. **Aloia RC, Jensen FC, Curtain CC, Mobley PW, Gordon LM.** 1988. Lipid composition and fluidity of the human immunodeficiency virus. Proc. Natl. Acad. Sci. U. S. A. **85:**900–904. http://dx.doi.org/10.1073/pnas.85.3.900.
26. **Chan R, Uchil PD, Jin J, Shui G, Ott DE, Mothes W, Wenk MR.** 2008. Retroviruses human immunodeficiency virus and murine leukemia virus are enriched in phosphoinositides. J. Virol. **82:**11228–11238. http://dx.doi.org/10.1128/JVI.00981-08.
27. **Julien JP, Huarte N, Maeso R, Taneva SG, Cunningham A, Nieva JL, Pai EF.** 2010. Ablation of the complementarity-determining region H3 apex of the anti-HIV-1 broadly neutralizing antibody 2F5 abrogates neutralizing capacity without affecting core epitope binding. J. Virol. **84:**4136–4147. http://dx.doi.org/10.1128/JVI.02357-09.
28. **Hope MJ, Bally MB, Webb G, Cullis PR.** 1985. Production of large unilamellar vesicles by a rapid extrusion procedure. Characterization of size distribution, trapped volume and ability to maintain a membrane potential. Biochim. Biophys. Acta **812:**55–65.
29. **Struck DK, Hoekstra D, Pagano RE.** 1981. Use of resonance energy transfer to monitor membrane fusion. Biochemistry **20:**4093–4099. http://dx.doi.org/10.1021/bi00517a023.
30. **Bagatolli LA, Sanchez SA, Hazlett T, Gratton E.** 2003. Giant vesicles, laurdan, and two-photon fluorescence microscopy: evidence of lipid lateral separation in bilayers. Methods Enzymol. **360:**481–500. http://dx.doi.org/10.1016/S0076-6879(03)60124-2.
31. **Phillips JC, Braun R, Wang W, Gumbart J, Tajkhorshid E, Villa E, Chipot C, Skeel RD, Kale L, Schulten K.** 2005. Scalable molecular dynamics with NAMD. J. Comput. Chem. **26:**1781–1802. http://dx.doi.org/10.1002/jcc.20289.
32. **MacKerell AD, Bashford D, Bellott Dunbrack RL, Evanseck JD, Field MJ, Fischer S, Gao J, Guo H, Ha S, Joseph-McCarthy D, Kuchnir L, Kuczera K, Lau FTK, Mattos C, Michnick S, Ngo T, Nguyen DT, Prodhom B, Reiher WE, Roux B, Schlenkrich M, Smith JC, Stote R, Straub J, Watanabe M, Wiórkiewicz-Kuczera J, Yin D, Karplus M.** 1998. All-atom empirical potential for molecular modeling and dynamics studies of proteins. J. Phys. Chem. B **102:**3586–3616. http://dx.doi.org/10.1021/jp973084f.
33. **Jorgensen WL, Chandrasekhar J, Madura JD, Impey RW, Klein ML.** 1983. Comparison of simple potential functions for simulating liquid water. J. Chem. Phys. **79:**926–935. http://dx.doi.org/10.1063/1.445869.
34. **Cournia Z, Smith JC, Ullmann GM.** 2005. A molecular mechanics force field for biologically important sterols. J. Comput. Chem. **26:**1383–1399. http://dx.doi.org/10.1002/jcc.20277.
35. **Martyna GJ, Tobias DJ, Klein ML.** 1994. Constant pressure molecular dynamics algorithms. J. Chem. Phys. **101:**4177–4189. http://dx.doi.org/10.1063/1.467468.
36. **Feller SE, Zhang Y, Pastor RW, Brooks BR.** 1995. Constant pressure molecular dynamics simulation: the Langevin piston method. J. Chem. Phys. **103:**4613–4621. http://dx.doi.org/10.1063/1.470648.
37. **Essmann U, Perera L, Berkowitz M.** 1995. A smooth particle mesh Ewald method. J. Chem. Phys. **103:**8577–8593. http://dx.doi.org/10.1063/1.470117.
38. **Miyamoto S, Kollman P.** 1992. Settle: an analytical version of the SHAKE and RATTLE algorithm for rigid water models. J. Comput. Chem. **13:**952–962. http://dx.doi.org/10.1002/jcc.540130805.
39. **Apellaniz B, Nir S, Nieva JL.** 2009. Distinct mechanisms of lipid bilayer perturbation induced by peptides derived from the membrane-proximal external region of HIV-1 gp41. Biochemistry **48:**5320–5331. http://dx.doi.org/10.1021/bi900504t.
40. **Sun ZY, Cheng Y, Kim M, Song L, Choi J, Kudahl UJ, Brusic V, Chowdhury B, Yu L, Seaman MS, Bellot G, Shih WM, Wagner G, Reinherz EL.** 2014. Disruption of helix-capping residues 671 and 674 reveals a role in HIV-1 entry for a specialized hinge segment of the membrane proximal external region of gp41. J. Mol. Biol. **426:**1095–1108. http://dx.doi.org/10.1016/j.jmb.2013.09.030.
41. **Lorizate M, Huarte N, Saez-Cirion A, Nieva JL.** 2008. Interfacial pretransmembrane domains in viral proteins promoting membrane fusion and fission. Biochim. Biophys. Acta **1778:**1624–1639. http://dx.doi.org/10.1016/j.bbamem.2007.12.018.
42. **Gangupomu VK, Abrams CF.** 2010. All-atom models of the membrane-spanning domain of HIV-1 gp41 from metadynamics. Biophys. J. **99:**3438–3444. http://dx.doi.org/10.1016/j.bpj.2010.09.054.
43. **Cohen T, Cohen SJ, Antonovsky N, Cohen IR, Shai Y.** 2010. HIV-1 gp41 and TCRalpha trans-membrane domains share a motif exploited by the HIV virus to modulate T-cell proliferation. PLoS Pathog. **6:**e1001085. http://dx.doi.org/10.1371/journal.ppat.1001085.
44. **Huarte N, Lorizate M, Maeso R, Kunert R, Arranz R, Valpuesta JM, Nieva JL.** 2008. The broadly neutralizing anti-human immunodeficiency virus type 1 4E10 monoclonal antibody is better adapted to membrane-bound epitope recognition and blocking than 2F5. J. Virol. **82:**8986–8996. http://dx.doi.org/10.1128/JVI.00846-08.
45. **Cardoso RM, Zwick MB, Stanfield RL, Kunert R, Binley JM, Katinger H, Burton DR, Wilson IA.** 2005. Broadly neutralizing anti-HIV antibody 4E10 recognizes a helical conformation of a highly conserved fusion-associated motif in gp41. Immunity **22:**163–173. http://dx.doi.org/10.1016/j.immuni.2004.12.011.
46. **Zwick MB, Jensen R, Church S, Wang M, Stiegler G, Kunert R, Katinger H, Burton DR.** 2005. Anti-human immunodeficiency virus type 1 (HIV-1) antibodies 2F5 and 4E10 require surprisingly few crucial residues in the membrane-proximal external region of glycoprotein gp41 to neutralize HIV-1. J. Virol. **79:**1252–1261. http://dx.doi.org/10.1128/JVI.79.2.1252-1261.2005.
47. **Frolov VA, Zimmerberg J.** 2010. Cooperative elastic stresses, the hydrophobic effect, and lipid tilt in membrane remodeling. FEBS Lett. **584:**1824–1829. http://dx.doi.org/10.1016/j.febslet.2010.01.039.
48. **Ivankin A, Apellaniz B, Gidalevitz D, Nieva JL.** 2012. Mechanism of membrane perturbation by the HIV-1 gp41 membrane-proximal external region and its modulation by cholesterol. Biochim. Biophys. Acta **1818:**2521–2528. http://dx.doi.org/10.1016/j.bbamem.2012.06.002.
49. **Aloia RC, Tian H, Jensen FC.** 1993. Lipid composition and fluidity of the human immunodeficiency virus envelope and host cell plasma membranes. Proc. Natl. Acad. Sci. U. S. A. **90:**5181–5185. http://dx.doi.org/10.1073/pnas.90.11.5181.
50. **McIntosh TJ, Simon SA.** 2007. Bilayers as protein solvents: role of bilayer structure and elastic properties. J. Gen. Physiol. **130:**225–227. http://dx.doi.org/10.1085/jgp.200709841.
51. **Needham D, Nunn RS.** 1990. Elastic deformation and failure of lipid bilayer membranes containing cholesterol. Biophys. J. **58:**997–1009. http://dx.doi.org/10.1016/S0006-3495(90)82444-9.
52. **Henriksen J, Rowat AC, Ipsen JH.** 2004. Vesicle fluctuation analysis of the effects of sterols on membrane bending rigidity. Eur. Biophys. J. **33:**732–741. http://dx.doi.org/10.1007/s00249-004-0420-5.
53. **Chen Z, Rand RP.** 1997. The influence of cholesterol on phospholipid membrane curvature and bending elasticity. Biophys. J. **73:**267–276. http://dx.doi.org/10.1016/S0006-3495(97)78067-6.
54. **Sarin PS, Gallo RC, Scheer DI, Crews F, Lippa AS.** 1985. Effects of a novel compound (AL 721) on HTLV-III infectivity in vitro. N. Engl. J. Med. **313:**1289–1290. http://dx.doi.org/10.1056/NEJM198511143132011.
55. **Schaffner CP, Plescia OJ, Pontani D, Sun D, Thornton A, Pandey RC, Sarin PS.** 1986. Anti-viral activity of amphotericin B methyl ester: inhibition of HTLV-III replication in cell culture. Biochem. Pharmacol. **35:**4110–4113. http://dx.doi.org/10.1016/0006-2952(86)90037-7.
56. **Graham DR, Chertova E, Hilburn JM, Arthur LO, Hildreth JE.** 2003. Cholesterol depletion of human immunodeficiency virus type 1 and simian immunodeficiency virus with beta-cyclodextrin inactivates and permeabilizes the virions: evidence for virion-associated lipid rafts. J. Virol. **77:**8237–8248. http://dx.doi.org/10.1128/JVI.77.15.8237-8248.2003.
57. **Guyader M, Kiyokawa E, Abrami L, Turelli P, Trono D.** 2002. Role for human immunodeficiency virus type 1 membrane cholesterol in viral internalization. J. Virol. **76:**10356–10364. http://dx.doi.org/10.1128/JVI.76.20.10356-10364.2002.
58. **Campbell SM, Crowe SM, Mak J.** 2002. Virion-associated cholesterol is critical for the maintenance of HIV-1 structure and infectivity. AIDS **16:**2253–2261. http://dx.doi.org/10.1097/00002030-200211220-00004.
59. **Vishwanathan SA, Thomas A, Brasseur R, Epand RF, Hunter E, Epand RM.** 2008. Hydrophobic substitutions in the first residue of the CRAC

segment of the gp41 protein of HIV. Biochemistry **47:**124–130. http://dx.doi.org/10.1021/bi7018892.
60. **Saez-Cirion A, Nir S, Lorizate M, Agirre A, Cruz A, Perez-Gil J, Nieva JL.** 2002. Sphingomyelin and cholesterol promote HIV-1 gp41 pretransmembrane sequence surface aggregation and membrane restructuring. J. Biol. Chem. **277:**21776–21785. http://dx.doi.org/10.1074/jbc.M202255200.
61. **van Meer G, Voelker DR, Feigenson GW.** 2008. Membrane lipids: where they are and how they behave. Nat. Rev. Mol. Cell Biol. **9:**112–124. http://dx.doi.org/10.1038/nrm2330.
62. **Kinnunen PK, Holopainen JM.** 2000. Mechanisms of initiation of membrane fusion: role of lipids. Biosci. Rep. **20:**465–482. http://dx.doi.org/10.1023/A:1010402819509.
63. **Larsson P, Kasson PM.** 2013. Lipid tail protrusion in simulations predicts fusogenic activity of influenza fusion peptide mutants and conformational models. PLoS Comput. Biol. **9:**e1002950. http://dx.doi.org/10.1371/journal.pcbi.1002950.
64. **Holopainen JM, Lehtonen JY, Kinnunen PK.** 1999. Evidence for the extended phospholipid conformation in membrane fusion and hemifusion. Biophys. J. **76:**2111–2120. http://dx.doi.org/10.1016/S0006-3495(99)77367-4.
65. **Sun ZY, Oh KJ, Kim M, Yu J, Brusic V, Song L, Qiao Z, Wang JH, Wagner G, Reinherz EL.** 2008. HIV-1 broadly neutralizing antibody extracts its epitope from a kinked gp41 ectodomain region on the viral membrane. Immunity **28:**52–63. http://dx.doi.org/10.1016/j.immuni.2007.11.018.
66. **Miyauchi K, Kim Y, Latinovic O, Morozov V, Melikyan GB.** 2009. HIV enters cells via endocytosis and dynamin-dependent fusion with endosomes. Cell **137:**433–444. http://dx.doi.org/10.1016/j.cell.2009.02.046.
67. **de la Vega M, Marin M, Kondo N, Miyauchi K, Kim Y, Epand RF, Epand RM, Melikyan GB.** 2011. Inhibition of HIV-1 endocytosis allows lipid mixing at the plasma membrane, but not complete fusion. Retrovirology **8:**99. http://dx.doi.org/10.1186/1742-4690-8-99.
68. **Melikyan GB.** 2014. HIV entry: a game of hide-and-fuse? Curr. Opin. Virol. **4:**1–7. http://dx.doi.org/10.1016/j.coviro.2013.09.004.
69. **Chen J, Frey G, Peng H, Rits-Volloch S, Garrity J, Seaman MS, Chen B.** 2014. Mechanism of HIV-1 neutralization by antibodies targeting a membrane-proximal region of gp41. J. Virol. **88:**1249–1258. http://dx.doi.org/10.1128/JVI.02664-13.
70. **Sanchez-Martinez S, Lorizate M, Katinger H, Kunert R, Nieva JL.** 2006. Membrane association and epitope recognition by HIV-1 neutralizing anti-gp41 2F5 and 4E10 antibodies. AIDS Res. Hum. Retroviruses **22:**998–1006. http://dx.doi.org/10.1089/aid.2006.22.998.
71. **Finton KA, Larimore K, Larman HB, Friend D, Correnti C, Rupert PB, Elledge SJ, Greenberg PD, Strong RK.** 2013. Autoreactivity and exceptional CDR plasticity (but not unusual polyspecificity) hinder elicitation of the anti-HIV antibody 4E10. PLoS Pathog. **9:**e1003639. http://dx.doi.org/10.1371/journal.ppat.1003639.
72. **Scherer EM, Leaman DP, Zwick MB, McMichael AJ, Burton DR.** 2010. Aromatic residues at the edge of the antibody combining site facilitate viral glycoprotein recognition through membrane interactions. Proc. Natl. Acad. Sci. U. S. A. **107:**1529–1534. http://dx.doi.org/10.1073/pnas.0909680107.
73. **Alving CR.** 2008. 4E10 and 2F5 monoclonal antibodies: binding specificities to phospholipids, tolerance, and clinical safety issues. AIDS **22:**649–651. http://dx.doi.org/10.1097/QAD.0b013e3282f51922.
74. **Alam SM, Morelli M, Dennison SM, Liao HX, Zhang R, Xia SM, Rits-Volloch S, Sun L, Harrison SC, Haynes BF, Chen B.** 2009. Role of HIV membrane in neutralization by two broadly neutralizing antibodies. Proc. Natl. Acad. Sci. U. S. A. **106:**20234–20239. http://dx.doi.org/10.1073/pnas.0908713106.
75. **Crooks GE, Hon G, Chandonia JM, Brenner SE.** 2004. WebLogo: a sequence logo generator. Genome Res. **14:**1188–1190. http://dx.doi.org/10.1101/gr.849004.